J. Cell. Mol. Med. Vol 16, No 5, 2012 pp. 1026-1037

# P2X7 purinoceptor alterations in dystrophic *mdx* mouse muscles: relationship to pathology and potential target for treatment

**Christopher N. J. Young [a], Wojciech Brutkowski [a], Chun-Fu Lien [a], Stephen Arkle [a], Hanns Lochmüller [b], Krzysztof Zabłocki [c], Dariusz C. Górecki [a, *]**

[a] *School of Pharmacy and Biomedical Sciences, University of Portsmouth, Portsmouth, UK*
[b] *Institute of Human Genetics, Newcastle University, Newcastle, UK*
[c] *Nencki Institute of Experimental Biology, Warsaw, Poland*

*Received: April 14, 2011; Accepted: July 14, 2011*

## Abstract

Duchenne muscular dystrophy (DMD) is a lethal inherited muscle disorder. Pathological characteristics of DMD skeletal muscles include, among others, abnormal $Ca^{2+}$ homeostasis and cell signalling. Here, in the *mdx* mouse model of DMD, we demonstrate significant P2X7 receptor abnormalities in isolated primary muscle cells and cell lines and in dystrophic muscles *in vivo*. P2X7 mRNA expression in dystrophic muscles was significantly up-regulated but without alterations of specific splice variant patterns. P2X7 protein was also up-regulated and this was associated with altered function of P2X7 receptors producing increased responsiveness of cytoplasmic $Ca^{2+}$ and extracellular signal-regulated kinase (ERK) phosphorylation to purinergic stimulation and altered sensitivity to NAD. $Ca^{2+}$ influx and ERK signalling were stimulated by ATP and BzATP, inhibited by specific P2X7 antagonists and insensitive to ivermectin, confirming P2X7 receptor involvement. Despite the presence of pannexin-1, prolonged P2X7 activation did not trigger cell permeabilization to propidium iodide or Lucifer yellow. In dystrophic mice, *in vivo* treatment with the P2X7 antagonist Coomassie Brilliant Blue reduced the number of degeneration–regeneration cycles in *mdx* skeletal muscles. Altered P2X7 expression and function is thus an important feature in dystrophic *mdx* muscle and treatments aiming to inhibit P2X7 receptor might slow the progression of this disease.

**Keywords:** P2X7 • Duchenne muscular dystrophy • *mdx* • $Ca^{2+}$ influx • ERK signalling • purinoceptor

## Introduction

Duchenne muscular dystrophy (DMD) is the second most common inherited disorder in man, and invariably leads to severe disability and premature death of young adults. This disease is caused by mutations of the DMD gene resulting in the absence or abnormalities of dystrophin. This protein, together with the dystrophin-associated protein complex, has a role in strengthening the sarcolemma during contractile activity [1]. However, additional pathogenic mechanisms are also involved. Intracellular free calcium $[Ca^{2+}]_i$ is raised in the sub-sarcolemmal region of dystrophic muscle, which cannot be explained by membrane ruptures alone [2].

We have previously shown that dystrophin appears to have a function in controlling purinergic responses. In dystrophic (*mdx*) mouse myoblasts, a purinergic phenotype arises in which exposure to extracellular ATP triggers an increase in cytosolic free calcium $[Ca^{2+}]_c$ caused primarily by activation of P2X7 receptors [3]. This receptor is an ATP-gated ion channel permeable to small cations, including $Ca^{2+}$, and its expression and/or function are up-regulated by inflammatory mediators and by ATP itself. The P2X7 receptor is therefore considered a 'danger' sensor, detecting ATP released where tissue damage occurs [4]. The intracellular ATP content of muscles is high and ATP, released in small amounts in response to physiological muscle activity, acts through purinergic receptors to modulate skeletal muscle plasticity [5]. In DMD, due to the fragility of myofibres, ATP is released

*Correspondence to: Dariusz C. GORECKI,
Harvard Medical School, Department of Cancer Biology,
Dana-Farber Cancer Institute, 450 Brookline Avenue,
Boston, MA 02215, USA.
Tel.: +44 239 284 3566, Fax: +44 239 284 3565
E-mail: darek.gorecki@port.ac.uk

doi:10.1111/j.1582-4934.2011.01397.x

in very large amounts into the extracellular space. These high concentrations of ATP, especially if acting on an altered receptor, could contribute to DMD pathology.

In this study, we show that P2X7 receptor expression and function are significantly altered in mouse dystrophic myoblasts and myotubes *in vitro* and *ex vivo* and also in *mdx* muscle *in vivo*. Pharmacological inhibition of this receptor in *mdx* mice *in vivo* resulted in a significantly lower number of revertant fibres in skeletal muscles, where such suppression is indicating a reduced number of degeneration–regeneration cycles in treated animals and used as one of the histological indicators for the assessment of therapeutic effects [6]. These data suggest that treatment with P2X7 antagonists may retard the dystrophic process.

# Materials and methods

## Animals

C57BL10 and *mdx* male mice were used in accordance with approvals of the institutional Ethical Review Board and the UK Home Office. Mice (3–9 per group) received 125 mg/kg b.w. Coomassie Brilliant Blue G 250 (Sigma-Aldrich, Gillingham, UK) i.p., in sterile saline, every three days from 3 to 14 weeks of age. Control mice received the same volume of saline solution. At 16 weeks, mice were killed and organs immediately frozen in isopentane cooled in liquid $N_2$ or placed in ice-cold homogenization buffer for protein or RNA extraction.

## Cell cultures

Normal (IMO) and *mdx* dystrophic (SC5) myoblast cell lines derived from adult male 'immorto' mice were cultured as previously described [3]. Their myogenic origins were confirmed (Fig. S1A). Myoblast to myotube differentiation (movie S1) was induced by substituting Foetal Bovine Serum (FBS) with 10% (v/v) HS, removal of γ-interferon and raising the incubation temperature to 37°C. J774 cells were maintained as previously described [7]. Primary cell cultures: freshly dissected soleus muscles from 4-month-old male C57Bl10 and *mdx* mice were used as previously described [8, 9] but with several modifications: cultures of proliferating primary myoblasts were established in Matrigel-coated cell culture plates (2 mg/ml reduced growth factor Matrigel; BD Biosciences, Oxford, UK) in a growth medium containing 20% (v/v) KSR (Knockout Serum Replacement; Invitrogen, Paisley, UK), 10% (v/v) Donor Horse Serum (Sera Labs, Haywards Heath, UK) and 2 mM L-glutamine. Contaminating non-muscle cells were removed by washing isolated fibres in three changes of fresh growth media and then by pre-plating and agitation to remove the myogenic cells before plating those on Matrigel. Resulting primary cells were harvested for immunohistochemistry or Western blot analyses.

## Antibodies

The following antibodies were used: P2X7-177003, rabbit polyclonal (Synaptic Systems, Goettingen, Germany), immunohistochemistry (IH) and Western blotting (WB) at 1:500 dilution; dystrophin: 2166, rabbit polyclonal (gift from D.J. Blake, Cardiff, UK) IH 1:500; dystrophin: 7A10, mouse monoclonal (DSHB) WB 1:100; extracellular signal-regulated kinase (ERK1/2): 9102, rabbit polyclonal (Cell Signalling Tech, Boston, USA) WB 1:2000; P-ERK1/2: 9106, mouse monoclonal (Cell Signalling Tech) WB 1:1000; F4/80: 74383, rabbit polyclonal (Abcam, Cambridge, UK) WB 1:500; β-actin: A2066, rabbit polyclonal (Sigma-Aldrich) WB, 1:100.

## RT-PCR analysis

Total cellular RNA was extracted from mouse skeletal muscle and muscle cell cultures using Trizol (Sigma-Aldrich) and first strands prepared using Superscript III first strand synthesis system (ThermoFisher, Loughborough, UK). Reverse transcriptase was omitted in negative controls. RT-PCRs for specific P2X7(a) and (k) variants were performed individually and in multiplex PCR. Exon 1a- and 1k-specific forward primers (5′-CACATGATCGTCTTTTCCTAC-3′ and 5′-GCCCGTGAGCCACTTATGC-3', respectively) were combined with reverse primers in exon 4 (5'-GGTCAGAAGAGCACTGTGC-3′), exon 5 (CCTTGTCTTGTCATATGGAAC-3′) or exon 7 (5′-TCTGTAAAGTTCTCTCCTGC-3′). Consistent results were obtained with different sets of primers. For exons 7–9 splicing the following primers were used: forward (e7–8) 5′-CTTTACAGAGGTGGCAGTTCAGGG-3′ or (e7–9) 5′-GAGAACTTTACAGAGGTGGCAGTTCAGATA-3′ with a common reverse primer 5′-CGAAGTAGGACAGGGTGGATCC-3′. PCR conditions were: 94°C for 10 sec., 57°C for 60 sec., and 72°C for 60 sec. followed by 72°C for 10 min.

Pannexin 1 primers were: 5′-GACTGGAGCTGGCGGTGGACAAGAT and 5′-GCGATCGGGGATGGTGCTGTCATTT-3′. PCR conditions were: 94°C for 10 sec., annealing 60°C for 60 sec. and extension 72°C for 60 sec. followed by 72°C for 10 min. PCR products were analysed in 2% (w/v) agarose gels and visualized using CHEMI GENIUS$^2$ BIO imaging system (Syngene, Cambridge, UK). PCR conditions and GAPDH controls were as previously described [3, 10]. The authenticity of PCR products was confirmed by restriction enzyme analysis or sequencing.

## Quantitative (Taq man qPCR) and semi-quantitative (sqPCR) analyses

qPCRs were performed using ABI Prism 7700 sequence detection system (PerkinElmer Life Sciences, Cambridge, UK) with Taqman probes. Relative expression was calculated as a ratio of P2X7 to GAPDH. Primers (Mm01199501_m1 to mouse P2X7 exon 3–4 and Mm00440582_m1, exons 5–6; mouse GAPDH endogenous control; Applied Biosystems) were used according to manufacturer's instructions. Semi-quantitative experiments to compare relative levels of P2X7(a) and P2X7(k) transcripts were performed essentially as previously described [11]. First-strand dilution series were used and 5 μl aliquots of PCR reactions were removed at cycle 14, 17, 20, 23 and 26 for GAPDH and 26, 29, 32, 35 and 40 for P2X7. PCR products were resolved by agarose gel electrophoresis and imaged following 2 sec. UV exposure using CHEMI GENIUS$^2$BIO imaging system (Syngene). Bands representing PCR products were quantified using the integrated pixel density measurement function of ImageJ software [12]. Integrated densities were plotted against cycle number to generate PCR profiles using non-linear curve fitting (Microcal Origin 7.0). $C_t$ values for GAPDH and P2X7 were derived from a standardized baseline and relative expression calculated as earlier. All experiments were repeated at least three times and performed in triplicate.

## Cytosolic $Ca^{2+}$ measurements in muscle cell lines *in vitro*

SC5 myoblasts were cultured in a 96-well plate for 48 hrs under conditions described in Materials and Methods. Cells (70–80% confluent) were loaded with 4 μM Fura 2-AM (Invitrogen) in culture medium for 35 min. at 37°C in a 95% $O_2$, 5% $CO_2$ atmosphere. After two brief washes in the assay buffer (132 mM NaCl, 5 mM KCl, 1 mM $MgCl_2$, 0.5 mM $Na_2HPO_4$, 1 mM sodium pyruvate, 5 mM D-glucose and 2 mM $CaCl_2$, 25 mM HEPES, pH 7.4) the plates were placed in the plate reader equipped with two injectors (POLARstar OPTIMA; BMG Labtech, Aylesbury, UK). Cells were treated first with 200 nM thapsigargin (Sigma-Aldrich) and then the effects of 1 mM ATP, in the absence or presence of ivermectin (IVM) or antagonists [13], were measured. Fluorescence was recorded at 510 nm with excitation at 340/380 nm. Each experiment was repeated at least three times.

## ERK1/2 phosphorylation assay

Cells were seeded at 50% confluency in 6-well collagen-coated plates (Greiner) in 2 ml of normal growth medium. After 24 hrs, growth medium was replaced with low serum medium (0.5%, v/v FBS). Cells were incubated for a further 24 hrs before application of agonists and antagonists. Agonists were applied for 10 min., and antagonists, where used, were applied 10 min. before the addition of agonists. Cells were lysed and extracted proteins used for immunoblot analysis with specific anti-p44/42 and anti-phosphop44/42 antibodies, as described later and in *SI* files.

## Western blotting

Proteins were extracted from adherent cells by scraping into extraction buffer Complete Lysis-M, 1 × Complete Protease Inhibitor Cocktail, 2 × PhosSTOP Phosphatase Inhibitor Cocktail (all Roche, London, UK), 2 mM sodium orthovanadate (Sigma-Aldrich) and homogenized by passing 20 times through a 23-gauge needle. Total proteins from frozen tissues were extracted by crushing samples in liquid nitrogen and further homogenization in extraction buffer (composition as earlier). All samples were centrifuged (800 × $g_{av}$ for 3 min. at 4°C) and protein concentrations determined using the bicinchonic acid assay kit (Sigma-Aldrich). Twenty micrograms of protein was mixed with Laemmli buffer at 1:1 (v/v) ratio with 2.5% (v/v) β-mercaptoethanol, heated for 5 min. at 95°C and chilled on ice. Samples were separated on 6–12% (w/v) SDS-PAGE and electroblotted onto Hybond C membranes (Amersham, UK). Blots were blocked in 5% (w/v) non-fat milk powder in 1× TBST, 0.01% (v/v) Tween-20 (Sigma-Aldrich) for 1 hr before probing with a primary antibody diluted in the same blocking buffer (overnight at 4°C or 2 hrs at RT), then washed (3×) with 1× PBST for 10 min. and incubated with the appropriate horseradish peroxidase-conjugated secondary antibody (Sigma-Aldrich) for 45 min. Specific protein bands were visualized using luminol-based substrates (Uptilight US; Cheshire Sciences, Chester, UK) and images obtained using a G:BOXChemi XT-16 system (Syngene). β-Actin antibody (Sigma-Aldrich) was used as a protein-loading control. All densitometric analyses of specific protein bands were made using exposure times within the linear range and the integrated density measurement function of ImageJ software [12]. All experiments were repeated at least three times with similar results obtained throughout.

# Protein deglycosylation assay

Protein samples (100 μg) were denatured in a buffer (5%, w/v SDS, 0.4M DTT) for 10 min. at 100°C, then samples were deglycosylated in the reaction buffer containing 2500U PNGaseF (New England Biolabs), 0.5M sodium phosphate, 10% (w/v) NP-40, for 1 hr at 37°C. Fifteen micrograms of digested samples were used for immunoblotting with anti-P2X7 antibody, as described earlier.

## Analysis of P2X7-dependent pore formation

Mouse myoblasts (SC-5, IMO) or macrophages (J774) were plated onto six-well plates (Nunc) coated with collagen and grown for 24 hrs. For the dye uptake assay, cells were incubated in HEPES buffer (composition as under $Ca^{2+}$ measurements above, with or without addition of 2 mM $CaCl_2$ or with substitution of NaCl by 130 mM K-glutamate) containing 50 μM propidium iodide (PI) or 3 mM Lucifer yellow. Following addition of 3–10 mM ATP, PI uptake was measured over 30 min. using an LSM 510 Meta microscope (Zeiss, London, UK). Fifty μg/ml digitonin was added at the end of each experiment to non-selectively permeabilize all cells. Sequential images were taken before addition of ATP, after 30 min. of incubation in the presence/absence of ATP and after addition of digitonin.

## Immunostaining

Cultured cells were fixed in 4% (w/v) paraformaldehyde (PFA) in 1× PBS for 15 min. at 4°C then endogenous peroxidase activity quenched in 1% (v/v) $H_2O_2$ in methanol for 15 min. on ice. Blocking was carried out in the appropriate normal serum [10% (v/v) in 1× PBS with 0.1% (v/v) Triton X-100 for 30 min. at RT] followed by avidin and biotin blocking solutions (Vector Laboratories, Peterborough, UK). Samples were incubated overnight at 4°C or at RT for 2 hrs with specific primary antibodies [diluted in 1× PBS with 10% (v/v) normal serum], washed and incubated with the respective biotinylated secondary antibody [Vector Laboratories; 1:200 with 2% (v/v) normal serum in 1× PBS] for 45 min. at RT. Three 5 min. washes in 1× PBST were used between each step. Staining was visualized using alkaline phosphatase substrate Vectastain® ABC-AP kit (Vector Laboratories), briefly rinsed in distilled water before nuclear counterstaining with methyl green (5 min.), then dehydrated and mounted using DPX.

## Histological muscle examinations

Immunolocalization of the revertant fibres was performed on 10-μm-thick muscle cryostat sections with the 2166 dystrophin antibody (1:500) in PBST containing 2% (v/v) goat serum and visualized *via* histochemical detection using Vectastain® ABC-AP kit (Vector Laboratories) as described earlier. Central nucleation was visualized by methyl green staining. Slides were dehydrated and mounted using DPX. Muscle section images were assembled as macro-images (Corel PHOTO-PAINT x3) and enumerations of revertant and centrally nucleated fibres were obtained *via* binary label-based counting using ImageJ Cell Counter Plugin [12]; two cross-sectional areas were assessed per muscle, taken at one third and two thirds longitudinal position, values were compared with total fibre counts per cross-section.

### Statistical analysis

Statistical significance of data was assessed using one- or two-way ANOVA with *post-hoc* Tukey's test (Microcal Origin 7.0) or Bonferonni test (Prism 4), respectively. A *P*-value of $< 0.05$ was considered statistically significant. Data are reported as mean $\pm$ S.E., where $n = 3$–5 for PCR and Western data and $n = 3$–9 for histological analyses.

## Results

### Expression of specific P2X7 mRNA splice variants in normal and dystrophic muscles

As the altered responses in dystrophic muscle cells *in vitro* [3] could not be explained by differences in the agonist concentrations used, there might be cell type–dependent variation in the molecular composition of the P2X7 receptor complex. P2X7 mRNA undergoes alternative splicing and splice variants have been identified for both the human and mouse P2X7, which significantly alter the receptor function [10, 14]. We have recently been involved in identification of a novel mouse P2X7 splice variant, P2X7(k), encoding an isoform that forms receptors with higher agonist sensitivity [10]. Therefore, RT-PCR analysis was performed to identify potential changes in the expression of specific P2X7 splice variants in dystrophic muscle. We first compared the expression patterns of the main P2X7(a) and the P2X7(k) variant in normal control (IMO, C57-immortalized) and dystrophic (SC5, *mdx*-immortalized) myoblast cultures and in normal and *mdx* adult muscles and brains. Both transcripts were detected in the IMO and SC5 myoblasts (Fig. 1) and in normal and dystrophic muscles and brains. Multiplex PCRs performed using both the P2X7(a) and (k) variant-specific forward primers and a common reverse primer indicated that there were no significant shifts in expression patterns or major differences in the relative amount of these splice variants in normal and dystrophic myoblasts and tibialis anterior (TA) muscles (Fig. 1B).

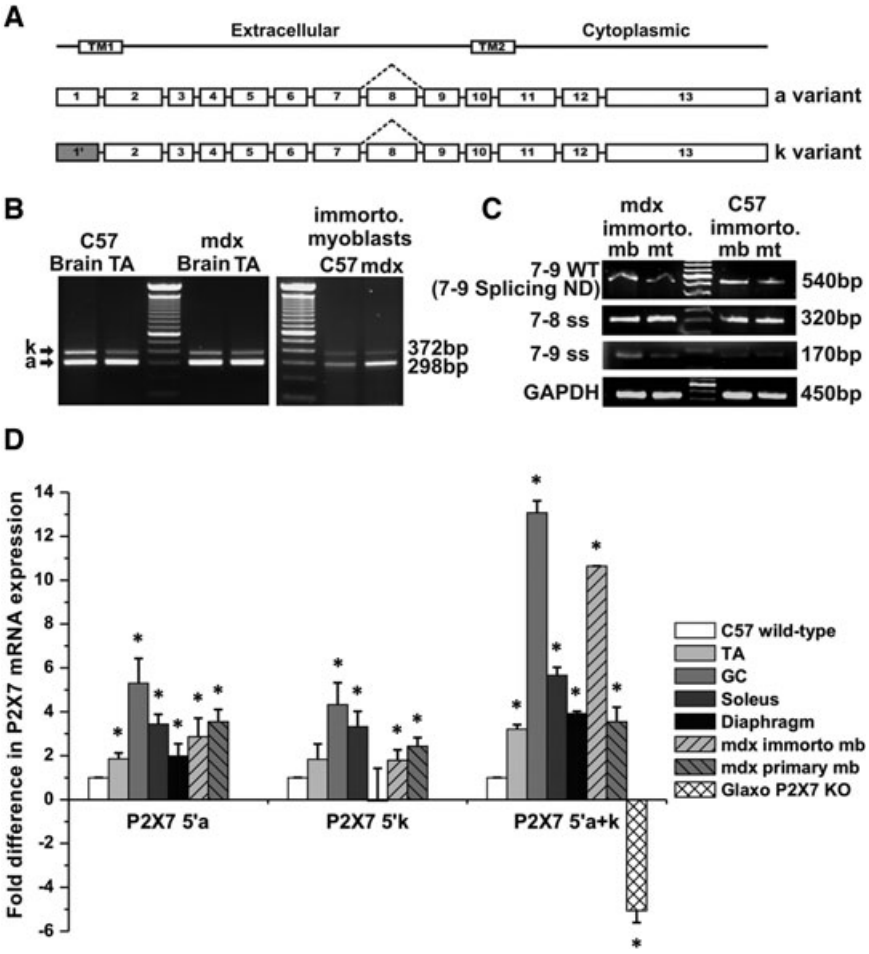


**Fig. 1** Characterization of P2X7 mRNA splice variant expressions in normal and dystrophic tissues. (**A**) Schematic illustration of the alternative exon 1 and exons 7–9 splice variants. (**B**) Representative images of PCR products visualized in agarose gels showing expression patterns of P2X7(a) and P2X7(k) variants in brain and TA muscle and in immortalized myoblasts derived from normal (C57) and *mdx* mouse skeletal muscle. (**C**) Representative gel images demonstrating the exons 7–9 splice variant presence (7–9ss). (**D**) Plot of qPCR data of total P2X7 mRNA expression in both wild-type and *mdx* immorto and primary myoblasts and in *mdx* muscles (TA, GC soleus and diaphragm) compared with normal controls ($^*P < 0.0001$, $F = 135.39$) and TA of Glaxo P2X7 splice-variant knockout mice. Each qPCR was repeated in at least three different samples and run in triplicates. Data were analysed by one-way ANOVA followed by Tukey's *post-hoc* test; error bars represent S.E.

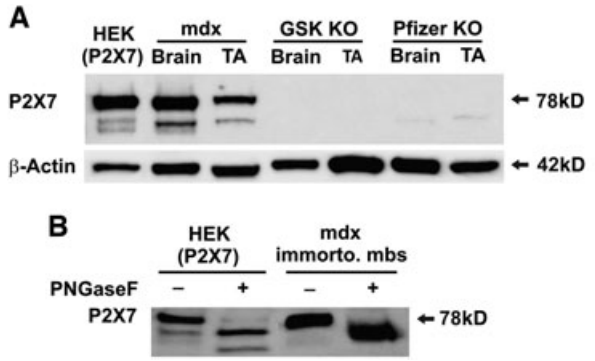


**Fig. 2** Characterization of P2X7 protein detection specificity. (**A**) Representative image of Western blot analysis with P2X7 antibody (Synaptic Systems) in protein samples from HEK cells overexpressing P2X7R, in brains and TA muscles from *mdx* mouse and from two P2X7 knockout strains (Glaxo and Pfizer). Distinct bands of ~78 kD are visible in protein samples from cells overexpressing P2X7R and in brain and muscle from *mdx* mouse but not in knockout samples. The specificity of smaller bands is unclear. (**B**) PNGase F deglycosylation reduced the main band size to ~65 kD in both P2X7R transfected HEK cells and in dystrophic myoblasts; $n = 3$.

Another alternatively spliced variant of the human P2X7 receptor lacking exon 8 and producing an isoforms with deleted C-terminus was shown to act in a dominant negative fashion to disrupt the normal ATP signalling in cancer cells [15]. We have analysed expression of a mouse orthologue of this splice variant in myoblasts and myotubes using primer sets spanning the spliced region (7+8+9) as well as primers specifically targeting the splice junctions (7/8 and 7/9). We found that this splicing event does occur in mice. However, the levels of the exons 7–9 splice variant were very low and there was no significant difference in its expression in normal *versus* dystrophic myoblasts or myotubes (Fig. 1C).

Next, real-time PCR (qPCR) was used to quantify differences in the relative abundance of the main P2X7 transcripts in dystrophic and normal muscles (Fig. 1D). Taqman analysis of global P2X7 expression levels in dystrophic and normal muscle showed significant up-regulation (3- to 14-fold) of this receptor mRNA in both immortalized and *mdx*-derived primary myoblasts and in dystrophic TA, gastrocnemius (GC), soleus and diaphragm muscles *in situ* (Fig. 1D; $P < 0.001$). Changes in primary cells and tissues ruled out the possibility that P2X7 up-regulation was an artefact of cell immortalization. In initial semi-quantitative experiments, exons 2–6 amplifications from first-strand dilution series established an expected increase in threshold cycle and showed that the $C_t$ values provide reliable estimates of relative P2X7 mRNA abundance. This was confirmed by using P2X7 splice variant knockout samples (Fig. 1D). Subsequently, semi-quantitative PCR analyses with specific primer sets revealed that both P2X7(a) and P2X7(k) transcripts were up-regulated to similar extents in all but one *mdx* muscle groups tested (Fig. 1D). The exception was *mdx* diaphragm, where the P2X7(a) increase was not associated with P2X7(k) variant up-regulation. The results of all qPCRs are summarized in Figure 1D.

## P2X7 receptor expression and signalling in normal and dystrophic myoblasts

Having shown increased expression of P2X7 transcripts in dystrophic cells and tissues, we analysed P2X7 protein levels in normal and dystrophic samples using Western blotting. Previous studies have shown that several of the available and commonly used antibodies are not fully specific to P2X7 proteins [16]. Our own analyses on HEK cells overexpressing P2X7 and in tissues (spleen, salivary glands, lungs, brains, kidneys, liver and skeletal muscle) from two P2X7 knockout mouse strains (Glaxo and Pfizer) revealed that, of several antibodies tested, the C-terminal antibody (Synaptic Systems) gave the most reproducible results under the conditions described here. This antibody was also suitable for detecting the main receptor splice variants [17]. Upon muscle sample separation by SDS-PAGE and immunoblotting, there was a predominant band at about 78 kD, the expected molecular mass of the glycosylated form of the P2X7 subunit (Figs 2A and 3A). Complete deglycosylation with PNGase F reduced the band size to ~65 kD, in good agreement with the calculated molecular weight of the protein (Fig. 2B). Bands of identical size and glycosylation patterns were detected in control protein extracts from HEK cells expressing mouse P2X7 protein and from dystrophic myoblasts (Figs 2B and 3A).

Comparison of protein samples from normal and dystrophic immortalized myoblasts showed a pronounced up-regulation of P2X7 protein in dystrophic cells (Fig. 3A), which was in agreement with higher transcript levels found in our qPCR data. Elevated levels of P2X7 receptor protein were also found in dystrophic myotubes (Fig. 3B).

Again, to exclude the possibility that P2X7 protein up-regulation was an artefact of cell immortalization, we analysed primary myoblasts from normal and *mdx* muscles. The results of these experiments confirmed a statistically significant ($P < 0.001$) increase in P2X7 protein in primary *mdx* myoblasts in comparison with non-dystrophic control (Fig. 3C). Increased P2X7 expression in primary *mdx* myoblasts detected by Western blotting correlated with qPCR (discussed earlier) and immunocytochemistry data (Fig. S1).

We previously demonstrated a significant increase of P2X7-mediated $Ca^{2+}$ influx in *mdx* myoblasts, which was blocked by two P2X7 receptor antagonists, Coomassie Brilliant Blue G-250 (CBB) and KN-62 [3]. Here, we have extended that study by using two novel P2X7 receptor antagonists; A740003 and A438079 of higher sensitivity and selectivity, which completely blocked $Ca^{2+}$ influx in a dose-dependent manner (Fig. 4). In addition to P2X7, expression of P2X4 receptors has previously been demonstrated in myoblasts [3] and recent evidence indicates specific structural

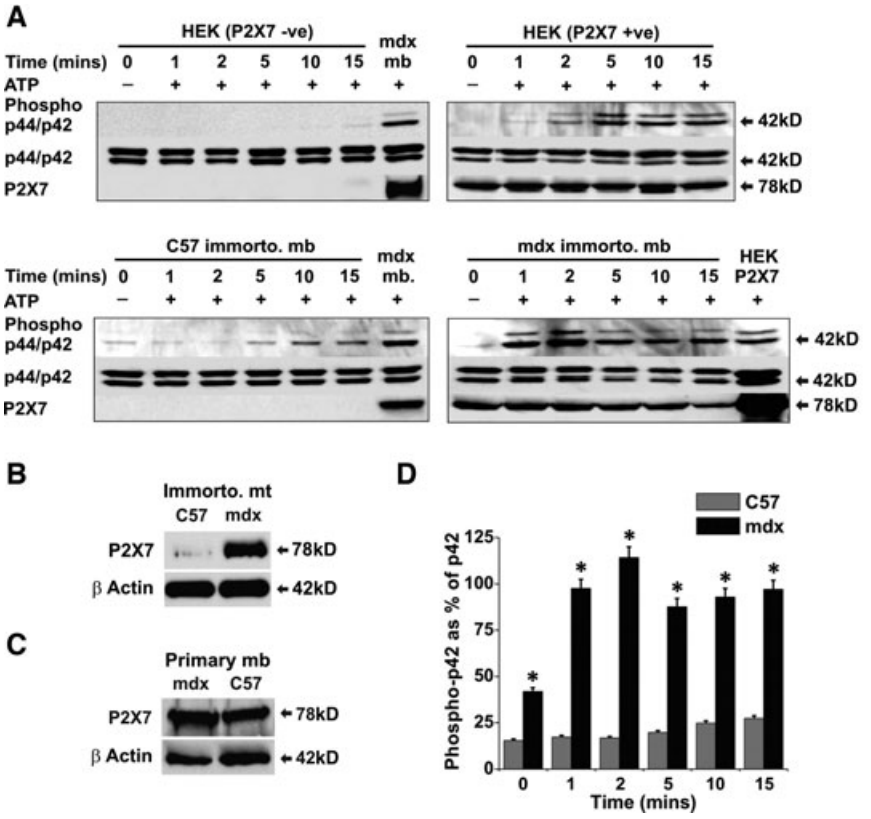


**Fig. 3** Analysis of P2X7R protein levels and ERK activation in normal and dystrophic muscle cells *in vitro*. (**A**) Representative immunoblots showing relative levels of phospho-p44/42, p44/42 and P2X7 receptor proteins at specific time-points (0–15 min.) following activation of P2X7R with 1 mM ATP. Top: HEK cells (negative controls) and HEK overexpressing P2X7 receptor (positive control); bottom: wild-type and *mdx* immorto myoblasts. Specific P2X7 receptor expressions and the extent of the time-dependent increase in ERK phosphorylation are shown. (**B**) Typical immunoblot showing P2X7 receptor levels in myotubes formed by dystrophic and control muscle cells. (**C**) Representative Western blot image of P2X7R levels in primary *mdx* and wild-type (C57) myoblasts. (**D**) Time course of phospho-p42 ERK induction in wild-type and *mdx* immorto myoblasts. Data from at least three independent experiments were quantified and plotted as means ± S.E.M. Statistical analysis performed with ANOVA with *post-hoc* Tukey's test demonstrated a significant effect ($*P < 0.001$) of cell type.

and functional interactions between P2X7 and P2X4 receptors [17]. However, pre-incubation of dystrophic myoblasts with 0.25 μM IVM, the allosteric P2X4 receptor modulator [18] did not potentiate $Ca^{2+}$ responses to ATP (Fig. 4).

Subsequently, we have analysed differences in ERK1/2 phosphorylation [19] as a marker of P2X7 signalling cascade independent of the $Ca^{2+}$ influx [20]. Western blotting with anti-ERK1/2 (p44/42) and anti-phosphoERK1/2 antibodies showed that dystrophic myoblasts responded to ATP with a sustained phosphorylation of these ERK proteins. This response was significantly faster and stronger than in normal myoblasts and showed correlation with P2X7 up-regulation (Fig. 3A and D). ERK phosphorylation in dystrophic cells was confirmed to be P2X7 dependent through the use of specific agonists and antagonists. The P2X7 agonist BzATP (300 μM) mimicked the effects of ATP (Fig. 5A) and a 10 min. pre-incubation with 1 μM CBB blocked the BzATP- and ATP-induced phospho-ERK response (Fig. 5A). Lower concentrations of ATP (25 μM) or pre-incubation of cells with 0.25 μM IVM before exposure to 500 μM ATP had no effect on ERK phosphorylation in dystrophic myoblasts (Fig. 5A), thus ruling out P2X4 receptors as having a significant role in these responses.

NAD is known to induce an ATP-independent activation of P2X7 receptors [21] and its effects have not been previously characterized in *mdx* muscles. Incubation of dystrophic myoblasts with 2 μM NAD caused a significant but transient ERK phosphorylation response (Fig. 5B). In contrast, 2 μM NAD was ineffective in control myoblasts or in HEK cells expressing homomeric P2X7(a) receptors (Fig. 5B).

## ATP does not induce cytolytic pore opening in dystrophic myoblasts

The sustained activation of P2X7 receptors triggers membrane permeabilization to large molecules up to 900 Da. We therefore tested whether or not activation of P2X7 could increase plasma membrane permeability in dystrophic cells. Initially, PI uptake was used to monitor ATP-induced large pore formation in proliferating dystrophic and control myoblasts and in J774 macrophages (positive control). Maximal cell permeabilization (100% cells) was measured as the nuclear dye influx following addition of 50 μg/ml digitonin. Addition of ATP triggered cell shape changes (rounding) in proliferating dystrophic myoblasts but ATP concentrations of 3–10 mM did not induce dye uptake into these cells in $Ca^{2+}$-containing medium, $Ca^{2+}$-free medium or in K-glutamate buffer (Fig. 6). Similarly, there was no discernible dye uptake into differentiating myoblasts (including C2C12 cells) or into differentiated myotubes (Fig. S2). In contrast, the same concentrations of ATP induced strong dye uptake into J774 macrophages (~99% positive

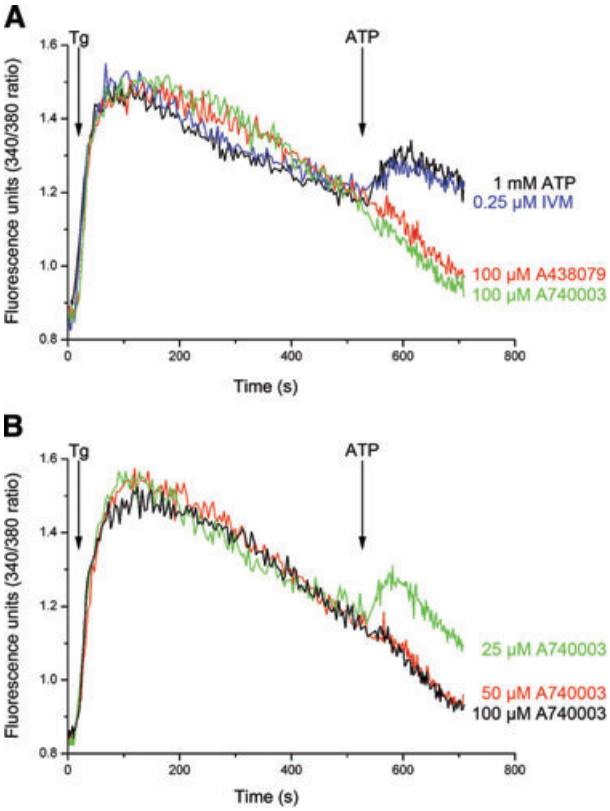


**Fig. 4** Characterization of receptors involved in ATP-evoked increases in $[Ca^{2+}]_c$ in immortalized *mdx* myoblasts. Reproducible traces generated by stimulation with ATP (1 mM) showing the effects of (**A**) ivermectin (IVM, 0.25 μM), A740003 and A438079 (both 100 μM). (**B**) The dose response effects of 25, 50 and 100 μM A740003 on ATP-stimulated responses. $T_g$ is the effect of thapsigargin (200 nM) pre-treatment used to empty intracellular $Ca^{2+}$ stores before addition of ATP in $Ca^{2+}$-containing medium. Traces are representative of three individual experiments conducted in triplicate.

cells; Fig. 6). A similar lack of permeabilizing response in dystrophic myoblasts was also observed with substitution of PI by the anionic dye, Lucifer yellow [22] (Fig. 6). The absence of pore opening was unlikely to be due to a lack of pannexin-1 channels [23] as RT-PCR amplification using pannexin-1 primers showed that both normal and dystrophic myoblasts and myotubes express this transcript, with relative levels being higher in undifferentiated cells (Fig. S3).

### Increased P2X7 receptor expression and signalling in normal and dystrophic muscles

To study P2X7 receptor protein in dystrophic muscles *in situ*, we performed Western blot analyses in muscle extracts from 4-month-old wild-type (C57Bl10) and dystrophic *mdx* mice (Fig. 7A and B). Densitometric analysis showed significant increases in P2X7 protein levels in *mdx* TA, GC, soleus and diaphragm muscles compared with age-matched wild-type controls (Fig. 7C). Importantly, concomitant with P2X7 up-regulation, there were significantly higher levels of phospho-ERK1/2 found in *mdx* mice muscles when compared to control samples (Fig. 7A and D).

At 4 months, inflammatory cell infiltrations in *mdx* leg muscles are decreased and thus would not be expected to contribute to P2X7 receptor levels [24]. However, to exclude the possibility that P2X7 protein levels were elevated due to its presence on residual macrophages, the same blots were re-probed with the pan-macrophage marker F4/80. No significant difference in F4/80 expression was found in *mdx* compared to wild-type muscle groups (Fig. 7E).

### Muscle analyses following CBB administration in *mdx* mice *in vivo*

To determine whether purinergic agents may influence the development of dystrophic phenotype *in vivo*, *mdx* mice were injected intraperitoneally with the P2X7 antagonist, CBB (125 mg/kg body weight) every 3 days over the vulnerable period (weeks 3–14) and analysed at 16 weeks. Control mice received the same volume of saline solution. Histological sections of TA muscle from these mice were analysed to determine the extent of central nucleation, total fibre number and revertant (dystrophin-positive) fibre counts. Both central nucleation and revertant fibre frequency increased with age, as expected (Fig. 8). However, there was a statistically significant decrease in the revertant fibre number in muscles of CBB-injected mice (Fig. 8), indicating a reduced number of degeneration–regeneration cycles [6] occurring in treated animals.

## Discussion

ATP is an important extracellular signalling molecule. Although first indications of functional ATP receptors in skeletal muscle cells emerged in 1983 [25], understanding of the physiological roles of these receptors has started to develop only recently. We know that extracellular ATP can potentiate excitation by acetylcholine at neuromuscular synapses [26, 27] and modulate $Ca^{2+}$ homeostasis and muscle plasticity [5]. In developing and regenerating skeletal muscles, ATP acting through two distinct classes of purinoceptors (P2X ionotropic and P2Y metabotropic receptors) has a role in myogenesis, satellite cell/myoblast proliferation, differentiation and motility [28–31], in neuromuscular junction formation [32, 33] or in muscle regeneration [34]. P2X7 has recently emerged as an important skeletal muscle receptor with roles in both activation of myoblast proliferation [28] and myotube formation [30] and in dystrophic pathologies [3, 35].

P2X7 expression and/or function are up-regulated by inflammatory mediators and by ATP itself [4] and are markedly increased in several pathologies [36, 37]. Results of this study demonstrate P2X7 purinergic alteration in myoblasts, differentiated myotubes

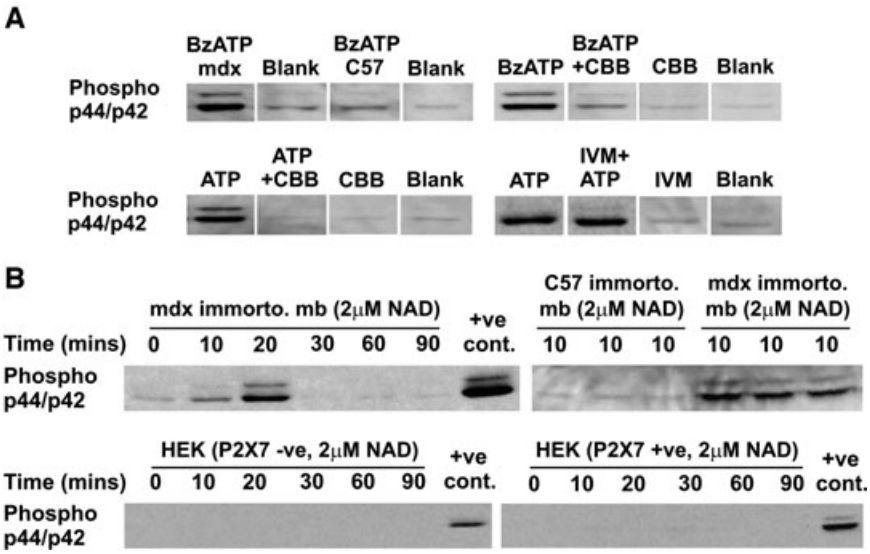


**Fig. 5** Characterization of P2X7 receptor activation in normal and dystrophic myoblasts. (**A**) Representative immunoblots showing changes in ERK phosphorylation studied using P2X7 agonist/antagonist combinations: BzATP (300 μM) and ATP (500 μM). CBB panels represent the effects of both agonists applied after10 min. pre-incubation with 1 μM CBB or with CBB alone (negative control). 0.25 μM ivermectin was used to study the potential involvement of P2X4 receptors. (**B**) Representative immunoblots of ERK phosphorylation triggered by 2 μM NAD. Note a transient ERK phosphorylation (top panels) in dystrophic myoblasts but not in wild-type cells (triplicate samples). NAD had no effect on ERK phosphorylation in HEK cells over-expressing P2X7R or in HEK controls (bottom right and left panels, respectively).

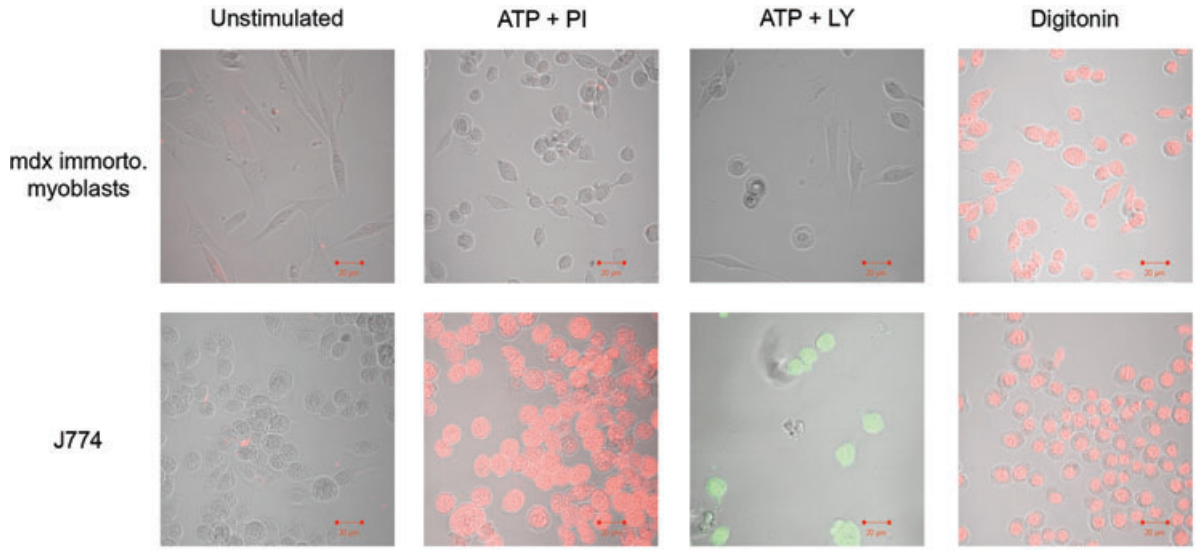


**Fig. 6** Absence of P2X7 cytolytic pore opening in *mdx* myoblasts. Propidium iodide (PI) and Lucifer yellow (LY) uptake following 30 min. stimulation with 10 mM ATP. Representative sequential images taken at the beginning of the experiment (unstimulated), after incubation with ATP in the presence of PI or LY and following total cell membrane permeabilization with digitonin are shown. ATP treatment caused significant PI fluorescence in J774 macrophages and triggered cell shape changes (rounding) in immortalised *mdx* myoblasts (SC5) but no PI or Lucifer yellow fluorescence. At least three independent experiments were performed with cells from three different early passages.

and in dystrophic *mdx* muscles *in situ* where we found both elevated levels of P2X7 mRNA and protein, as well as changes in receptor functions.

In view of significant differences in ATP sensitivities of recently discovered P2X7 splice variants, which could explain the dystrophic phenotype, we have compared these splicing patterns in normal and dystrophic samples. However, the P2X7(k) higher sensitivity variant [10] was only a minor P2X7 transcript in muscle cells and its up-regulation in dystrophic muscles (except diaphragms) mirrored that of the P2X7(a) variant. The mouse orthologue of a human P2X7 receptor transcript with exon 8 spliced out (and a resulting shift of coding frame) does exist. This truncated variant was previously found in human cancer cells, where it may block normal P2X7 functions [15]. However, it was a low-abundance transcript in muscles and its expression did not change in dystrophic cells. It would therefore seem unlikely that

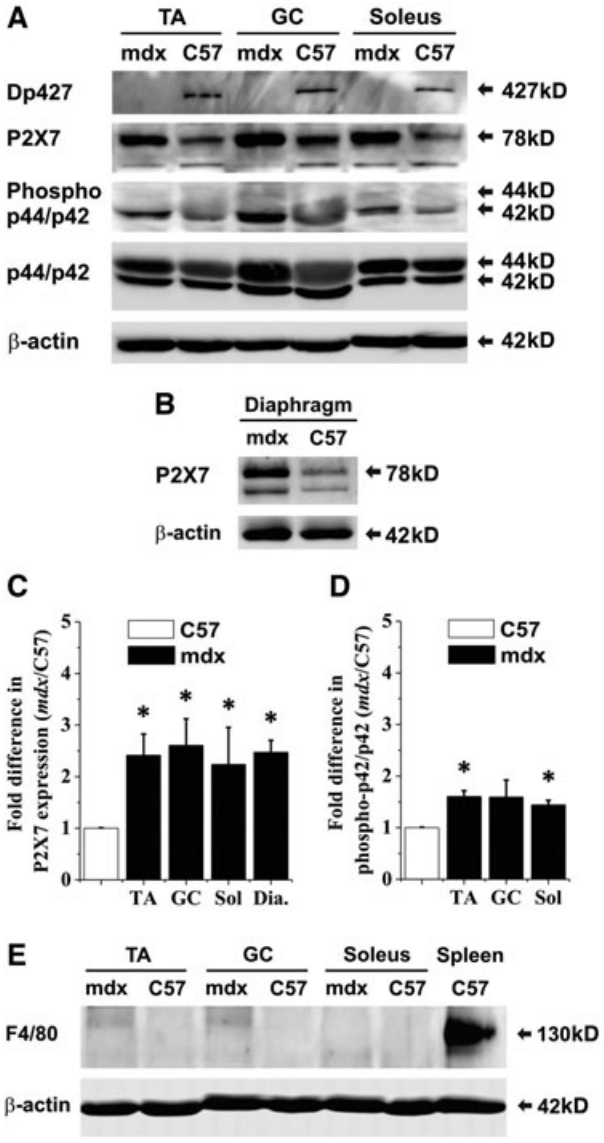


**Fig. 7** Analysis of P2X7 expression and activation in *mdx* and C57 muscles at 4 month. (**A**) Immunoblots of dystrophin (Dp427 muscle isoform), P2X7 receptor, ERK and phospho-ERK1/2 in protein extracts from hind limb muscles [tibialis anterior (TA), gastrocnemius (GC), soleus] and (**B**) in diaphragms of 4 month old wild-type and *mdx* mice. β-Actin represents a control for equal protein loading. Images are representative of at least three independent experiments. (**C**, **D**) Densitometric analyses of immunoblot results. Two-way ANOVA revealed that for P2X7 protein expression levels, the main effect of genotype was significant ($*P < 0.0001$, $F = 59.91$) whereas the effect of muscle type was not significant ($P > 0.05$). Moreover, for phospho-ERK1/2 protein expressed as a percentage of ERK1/2, the main effects of muscle type and genotype were significant ($*P = 0.0010$, $F = 12.88$ and $P = 0.0007$, $F = 20.15$, respectively). (**E**) Representative immunoblot analysis of the same set of leg muscle samples with the F4/80 macrophage marker to evaluate the abundance of macrophages in dystrophic muscles at 4 months of age.

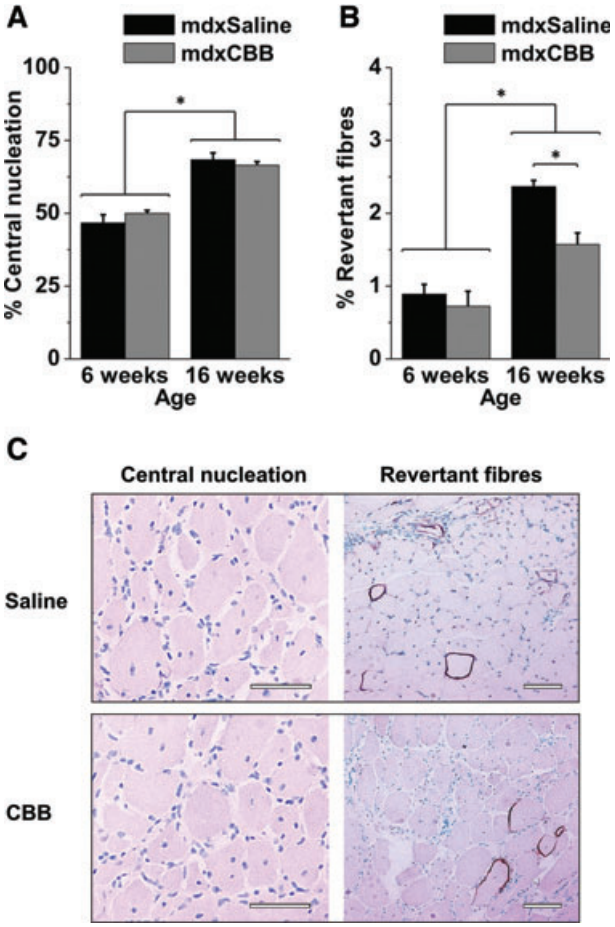


**Fig. 8** Analysis of *mdx* muscles following CBB administration *in vivo*. Relative proportion of centrally nucleated (**A**) and dystrophin-positive revertant fibres (**B**) in TA *mdx* muscles following treatment with CBB. There was an expected significant increase in numbers of centrally nucleated (**A**) and revertant fibres (**B**) with age ($*P < 0.05$). CBB treatment caused a statistically significant decrease in numbers of revertant fibres in 16-week-old *mdx* mice ($*P = 0.028$, $F = 5.799$); $n \geq 5$. Data were analysed using two-way ANOVA with *post-hoc* Bonferroni test. Error bars represent S.E. (**C**) Representative micrographs showing regions of central nucleation and revertant fibres (dystrophin immunolocalization; VIP staining) in saline- and CBB-injected animals (scale bars = 60 μm).

differences in the preponderance of these splice variants could explain the dystrophic P2X7 phenotype.

Stimulation of P2X7 receptors activates various cell signalling pathways including ERK1/2 phosphorylation and $Ca^{2+}$ fluxes. In dystrophic but not control muscle cells, both pathways were activated and showed specific agonist/antagonist dependencies, confirming these as being evoked by P2X7 receptor stimulation. The ERK pathway is known to have dual roles in muscles. It can inhibit differentiation at the onset but also promote fusion at the late stage of muscle

differentiation [38–40]. However, ERK phosphorylation can be triggered by a plethora of stimuli [41] and therefore the importance of P2X7 activation for ERK muscle function is currently not clear.

In addition to the more rapid ERK signalling associated with the dystrophic phenotype, there is also altered sensitivity to NAD [21], which confirms that the molecular *milieu* in which P2X7 signalling occurs differs between diseased and normal cells. Further studies should reveal the mechanism(s) linking dystrophin absence with P2X7 receptor function.

In muscle, as in other cells studied, ATP may have a dual role. Low, possibly tonic ATP concentrations having a signalling function leading to cell proliferation, migration or differentiation, while a sustained stimulation by high ATP concentrations may result in drastic changes in cellular homeostasis [42, 43].

The intracellular ATP content of muscle is particularly high and thus large amounts are released into the extracellular space due to the fragility of dystrophic myofibres. The P2X7 receptor is considered a 'danger' sensor, detecting ATP released where tissue damage occurs [4, 42, 44]. P2X7 activation affects the pro-inflammatory pathways [37] and the molecular signature of dystrophic muscle is dominated by an inflammatory response [45]. Recent data indeed showed a direct link between inflammation and P2X7 in dystrophic muscles. Skeletal muscle cells (myoblasts and myotubes) stimulated with P2X7 agonists actively participated in inflammasome formation and ASC-1, pro-IL-1β and pro-caspase-1 levels were up-regulated in the muscle tissue of dysferlin-deficient (LGMD-2B) and dystrophin-deficient mice [35]. In skeletal muscles, growth and regeneration are regulated by certain inflammatory mediators, for example IL-6, IL-4 [46]. Under physiological conditions pro-inflammatory roles of P2X7 receptors and their effects on muscle growth and regeneration might be positively linked but precisely controlled by receptor desensitization and ecto-ATPase activity. However, these highly regulated effects appear to be dysfunctional in dystrophic muscles.

Interestingly, our data show differences in ATP-evoked P2X7 receptor activation in dystrophic myoblasts. The purinergic phenotype occurring in myoblasts is an unexpected finding. This reflects the prevailing opinion that, because dystrophin protein in myoblasts is very low or absent, phenotypic consequences of mutation are unlikely to affect such cells. Contrary to this, Ferrari *et al*. (1994) showed that DMD lymphoblasts (cells with dystrophin protein also low or absent) are eminently more susceptible to ATP damage than their non-dystrophic counterparts [47] and we have shown [3] (and here) that myoblasts derived from the *mdx* mouse were more susceptible to nucleotide stimulation and also had abnormal energy metabolism [48]. In support of these findings, other functions including autonomous differentiation of dystrophic myoblasts/satellite cells [41] and dystrophic stem cell loss in early muscle formation [49] have been documented.

The mechanism(s) of P2X7-induced cell death are not fully understood and are cell-type dependent. In some cells prolonged P2X7 stimulation leads to apoptosis, in others it has characteristics of both necrosis and apoptosis. P2X7 receptors can, upon prolonged stimulation, trigger membrane permeability to large molecules (<900 Da), which is often a prelude to cell death. Interestingly, while both $Ca^{2+}$ influx and ERK phosphorylation were clearly enhanced in dystrophic muscle cells, we were not able to elicit either cationic or anionic [22] dye uptake (large pore opening) in these cells, whether as proliferating or differentiating myoblasts or as myotubes.

It has been suggested that pannexin-1 hemi-channels interact with P2X7 receptors to form a pore [23]. However, involvement of pannexin-1 is not always observed or necessary [50], consistent with our data showing no pore formation even though pannexin-1 transcript was expressed in both myoblasts and myotubes.

Nevertheless, irrespective of the mechanism involved, P2X7 responses may control an intricate equilibrium between cycles of muscle degeneration and regeneration in *mdx* mice.

Finally, DMD myotube damage is considered to be the result of an increased level of $[Ca^{2+}]_i$ [2]. We found increased expression and activity of P2X7 ion channel in dystrophic myotubes and muscles *in situ*. Furthermore, ATP-mediated membrane depolarization leads to the secondary modulation of voltage-gated $Ca^{2+}$channels while depletion of the internal $Ca^{2+}$ stores would also activate opening of the cell membrane $Ca^{2+}$ channels, according to the store-operated mechanism [42]. Importantly, altered $Ca^{2+}$ influx *via* L-type, TRP and stretch-activated channels has been observed in *mdx* myotubes [51–55] and medications decreasing $[Ca^{2+}]_i$ enhance survival of dystrophic muscles [2,56]. In the light of our data, therapies aimed at decreasing ATP stimulation should be assessed for potential benefit in DMD. Indeed, suramin (a broad P2 receptor antagonist) reduced *mdx* muscle damage [57, 58] and our data show a decrease of degeneration-regeneration cycles in *mdx* mice treated with a specific inhibitor CBB. If the same effects were found in human muscles this could be an important aspect of the treatment of this lethal disease.

## Acknowledgements

DCG holds the Fulbright Distinguished Scholarship. This work was supported by the Interreg IV (AdMiN) grant to DCG, the Institute of Biomedical and Biomolecular Sciences PhD grant to C.Y. and the Medical Research Council UK through the Centre for Neuromuscular Diseases (G0601943) to H.L. We thank Drs F. Koch-Nolte for providing HEK(P2X7R) cells, D. Blake for 2166 antibody, GlaxoSmithKline, Harlow, UK ,for the P2X7 knockout mice, G. Scarlett for advice on qPCR and J. Smith for help with the live cell imaging.

## Conflict of interest

The authors confirm that there are no conflicts of interest.

## Supporting Information

Additional Supporting Information may be found in the online version of this article:

**Fig. S1** Muscle cell characterization.

**Fig. S2** Absence of P2X7 cytolytic pore opening in muscle cells.

**Fig. S3** Expression of pannexin 1 in muscle cells.

**Movie S1** Myotubes *in vitro*.

Please note: Wiley-Blackwell is not responsible for the content or functionality of any supporting materials supplied by the authors. Any queries (other than missing material) should be directed to the corresponding author for the article.

## References


1. **Dalkilic I, Kunkel LM**. Muscular dystrophies: genes to pathogenesis. *Curr Opin Genet Dev*. 2003; 13: 231–8.
2. **Millay DP, Goonasekera SA, Sargent MA, *et al.*** Calcium influx is sufficient to induce muscular dystrophy through a TRPC-dependent mechanism. *Proc Natl Acad Sci USA*. 2009; 106: 19023–8.
3. **Yeung D, Zablocki K, Lien CF, *et al.*** Increased susceptibility to ATP *via* alteration of P2X receptor function in dystrophic mdx mouse muscle cells. *FASEB J*. 2006; 20: 610–20.
4. **Khakh BS, North RA.** P2X receptors as cell-surface ATP sensors in health and disease. *Nature*. 2006; 442: 527–32.
5. **Buvinic S, Almarza G, Bustamante M, *et al.*** ATP released by electrical stimuli elicits calcium transients and gene expression in skeletal muscle. *J Biol Chem*. 2009; 284: 34490–505.
6. **Yokota T, Lu QL, Morgan JE, *et al.*** Expansion of revertant fibers in dystrophic mdx muscles reflects activity of muscle precursor cells and serves as an index of muscle regeneration. *J Cell Sci*. 2006; 119: 2679–87.
7. **Coutinho-Silva R, Ojcius DM, Gorecki DC, *et al.*** Multiple P2X and P2Y receptor subtypes in mouse J774, spleen and peritoneal macrophages. *Biochem Pharmacol*. 2005; 69: 641–55.
8. **Rosenblatt JD, Lunt AI, Parry DJ, *et al.*** Culturing muscle cells from single living muscle fibre explants. *J Biol Chem*. 2009; 284: 25813–22.
9. **Rosenblatt JD, Lunt AI Parry DJ, *et al.*** *In vitro* cell. *Dev. Biol.-Animal* 2005; 31: 773–779.
10. **Nicke A, Kuan YH, Masin M, *et al.*** A functional P2X7 splice variant with an alternative transmembrane domain 1 escapes gene inactivation in P2X7 knockout mice. *J Biol Chem*. 2009; 284: 25813–22.
11. **Beresewicz M, Majewska M, Makarewicz D, *et al.*** Changes in the expression of insulin-like growth factor 1 variants in the postnatal brain development and in neonatal hypoxia-ischaemia. *Int J Dev Neurosci*. 2010; 28: 91–7.
12. **Abramoff MD, Magelhaes PJ, Ram SJ.** Image processing with Image. *J. Biophoton Int*. 2004; 11: 36–42.
13. **Donnelly-Roberts DL, Namovic MT, Han P, *et al.*** Mammalian P2X7 receptor pharmacology: comparison of recombinant mouse, rat and human P2X7 receptors. *Br J Pharmacol*. 2009; 157: 1203–14.
14. **Cheewatrakoolpong B, Gilchrest H, Anthes JC, *et al.*** Identification and characterization of splice variants of the human P2X7 ATP channel. *Biochem Biophys Res Commun*. 2005; 332: 17–27.
15. **Feng YH, Li X, Wang L, *et al.*** A truncated P2X7 receptor variant (P2X7-j) endogenously expressed in cervical cancer cells antagonizes the full-length P2X7 receptor through hetero-oligomerization. *J Biol Chem*. 2006; 281: 17228–37.
16. **Sim JA, Young MT, Sung HY, *et al.*** Reanalysis of P2X7 receptor expression in rodent brain. *J Neurosci*. 2004; 24: 6307–14.
17. **Masin M, Young C, Lim K, *et al.*** Expression, assembly and function of novel C-terminal truncated variants of the mouse P2X7 receptor: re-evaluation of P2X7 knockouts. *Br J Pharmacol*. 2011; in press: doi: 10.1111/j.1476-5381.2011.01624.x.
18. **Boumechache M, Masin M, Edwardson JM, *et al.*** Analysis of assembly and trafficking of native P2X4 and P2X7 receptor complexes in rodent immune cells. *J Biol Chem*. 2009; 284: 13446–54.
19. **Priel A, Silberberg SD.** Mechanism of ivermectin facilitation of human P2X4 receptor channels. *J Gen Physiol*. 2004; 123: 281–93.
20. **Budagian V, Bulanova E, Brovko L, *et al.*** Signaling through P2X7 receptor in human T cells involves p56lck, MAP kinases, and transcription factors AP-1 and NF-kappa B. *J Biol Chem*. 2003; 278: 1549–60.
21. **Amstrup J, Novak I.** P2X7 receptor activates extracellular signal-regulated kinases ERK1 and ERK2 independently of $Ca^{2+}$ influx. *Biochem J*. 2003; 374: 51–61.
22. **Hong S, Schwarz N, Brass A, *et al.*** Differential regulation of P2X7 receptor activation by extracellular nicotinamide adenine dinucleotide and ecto-ADP-ribosyltransferases in murine macrophages and T cells. *J Immunol*. 2009; 183: 578–92.
23. **Schachter J, Motta AP, de Souza Zamorano A, *et al.*** ATP-induced P2X7-associated uptake of large molecules involves distinct mechanisms for cations and anions in macrophages. *J Cell Sci*. 2008; 121: 3261–70.
24. **Vessey DA, Li L, Kelley M.** Pannexin-I/P2X 7 purinergic receptor channels mediate the release of cardioprotectants induced by ischaemic pre- and postconditioning. *J Cardiovasc Pharmacol Ther*. 2010; 15: 190–5.
25. **Yeung D, Kharidia R, Brown SC, *et al.*** Enhanced expression of the P2X4 receptor in Duchenne muscular dystrophy correlates with macrophage invasion. *Neurobiol Dis*. 2004; 15: 212–20.
26. **Kolb HA, Wakelam MJ.** Transmitter-like action of ATP on patched membranes of cultured myoblasts and myotubes. *Nature*. 1983; 303: 621–3.
27. **Vizi ES, Nitahara K, Sato K, *et al.*** Stimulation-dependent release, breakdown, and action of endogenous ATP in mouse hemidiaphragm preparation: the possible role of ATP in neuromuscular transmission. *J Auton Nerv Syst*. 2000; 81: 278–84.
28. **Lu Z, Smith DO.** Adenosine 5′-triphosphate increases acetylcholine channel opening frequency in rat skeletal muscle. *J Physiol*. 1991; 436: 45–56.
29. **Martinello T, Baldoin MC, Morbiato L, *et al.*** Extracellular ATP signaling during

differentiation of C2C12 skeletal muscle cells: role in proliferation. *Mol Cell Biochem*. 2011; 351: 183–96.

30. **Deli T, Toth BI, Czifra G, Szappanos H, *et al.*** Differences in purinergic and voltage-dependent signalling during protein kinase Calpha overexpression- and culturing-induced differentiation of C2C12 myoblasts. *J Muscle Res Cell Motil*. 2006; 27: 617–30.
31. **Araya R, Riquelme MA, Brandan E, *et al.*** The formation of skeletal muscle myotubes requires functional membrane receptors activated by extracellular ATP. *Brain Res Brain Res Rev*. 2004; 47: 174–88.
32. **Ryten M, Dunn PM, Neary JT, *et al.*** ATP regulates the differentiation of mammalian skeletal muscle by activation of a P2X5 receptor on satellite cells. *J Cell Biol*. 2002; 158: 345–55.
33. **Ryten M, Koshi R, Knight GE, *et al.*** Abnormalities in neuromuscular junction structure and skeletal muscle function in mice lacking the P2X2 nucleotide receptor. *Neuroscience*. 2007; 148: 700–11.
34. **Choi RC, Man ML, Ling KK, *et al.*** Expression of the P2Y1 nucleotide receptor in chick muscle: its functional role in the regulation of acetylcholinesterase and acetylcholine receptor. *J Neurosci*. 2001; 21: 9224–34.
35. **Jiang LH, Rassendren F, Mackenzie A, *et al.*** N-methyl-D-glucamine and propidium dyes utilize different permeation pathways at rat P2X(7) receptors. *Am J Physiol Cell Physiol*. 2005; 289: C1295–302.
36. **Rawat R, Cohen TV, Ampong B, *et al.*** Inflammasome up-regulation and activation in dysferlin-deficient skeletal muscle. *Am J Pathol*. 2010; 176: 2891–900.
37. **Skaper SD, Debetto P, Giusti P.** The P2X7 purinergic receptor: from physiology to neurological disorders. *FASEB J*. 2010; 24: 337–45.
38. **Di Virgilio F.** Liaisons dangereuses: P2X(7) and the inflammasome. *Trends Pharmacol Sci*. 2007; 28: 465–72.
39. **Coolican SA, Samuel DS, Ewton DZ, *et al.*** The mitogenic and myogenic actions of insulin-like growth factors utilize distinct signaling pathways. *J Biol Chem*. 1997; 272: 6653–62.
40. **Bennett AM, Tonks NK.** Regulation of distinct stages of skeletal muscle differentiation by mitogen-activated protein kinases. *Science*. 1997; 278: 1288–91.
41. **Wu Z, Woodring PJ, Bhakta KS, *et al.*** p38 and extracellular signal-regulated kinases regulate the myogenic program at multiple steps. *Mol Cell Biol*. 2000; 20: 3951–64.
42. **Rommel C, Clarke BA, Zimmermann S, *et al.*** Differentiation stage-specific inhibition of the Raf-MEK-ERK pathway by Akt. *Science*. 1999; 286: 1738–41.
43. **Surprenant A, North RA.** Signaling at purinergic P2X receptors. *Annu Rev Physiol*. 2009; 71: 333–59.
44. **Di Virgilio F, Ferrari D, Adinolfi E.** P2X(7): a growth-promoting receptor-implications for cancer. *Purinergic Signal*. 2009; 5: 251–6.
45. **Ponnusamy M, Ma L, Gong R, *et al.*** P2X7 receptors mediate deleterious renal epithelial-fibroblast cross talk. *Am J Physiol Renal Physiol*. 2011; 300: F62–70.
46. **Porter JD, Khanna S, Kaminski HJ, *et al.*** A chronic inflammatory response dominates the skeletal muscle molecular signature in dystrophin-deficient mdx mice. *Hum Mol Genet*. 2002; 11: 263–72.
47. **Serrano AL, Baeza-Raja B, Perdiguero E, *et al.*** Interleukin-6 is an essential regulator of satellite cell-mediated skeletal muscle hypertrophy. *Cell Metab*. 2008; 7: 33–44.
48. **Ferrari D, Munerati M, Melchiorri L, *et al.*** Responses to extracellular ATP of lymphoblastoid cell lines from Duchenne muscular dystrophy patients. *Am J Physiol*. 1994; 267: C886–92.
49. **Onopiuk M, Brutkowski W, Wierzbicka K, *et al.*** Mutation in dystrophin-encoding gene affects energy metabolism in mouse myoblasts. *Biochem Biophys Res Commun*. 2009; 386: 463–6.
50. **Merrick D, Stadler LK, Larner D, *et al.*** Muscular dystrophy begins early in embryonic development deriving from stem cell loss and disrupted skeletal muscle formation. *Dis Model Mech*. 2009; 2: 374–88.
51. **Yan Z, Li S, Liang Z, *et al.*** The P2X7 receptor channel pore dilates under physiological ion conditions. *J Gen Physiol*. 2008; 132: 563–73.
52. **Vandebrouck A, Ducret T, Basset O, *et al.*** Regulation of store-operated calcium entries and mitochondrial uptake by minidystrophin expression in cultured myotubes. *FASEB J*. 2006; 20: 136–8.
53. **Vandebrouck C, Martin D, Colson-Van Schoor M, *et al.*** Involvement of TRPC in the abnormal calcium influx observed in dystrophic (mdx) mouse skeletal muscle fibers. *J Cell Biol*. 2002; 158: 1089–96.
54. **Kumar A, Khandelwal N, Malya R, *et al.*** Loss of dystrophin causes aberrant mechanotransduction in skeletal muscle fibers. *FASEB J*. 2004; 18: 102–13.
55. **Iwata Y, Katanosaka Y, Arai Y, *et al.*** A novel mechanism of myocyte degeneration involving the Ca2+-permeable growth factor-regulated channel. *J Cell Biol*. 2003; 161: 957–67.
56. **Friedrich O, Both M, Gillis JM, *et al.*** Mini-dystrophin restores L-type calcium currents in skeletal muscle of transgenic mdx mice. *J Physiol*. 2004; 555: 251–65.
57. **Matsumura CY, Pertille A, Albuquerque TC, *et al.*** Diltiazem and verapamil protect dystrophin-deficient muscle fibers of MDX mice from degeneration: a potential role in calcium buffering and sarcolemmal stability. *Muscle Nerve*. 2009; 39: 167–76.
58. **Taniguti AP, Pertille A, Matsumura CY, *et al.*** Prevention of muscle fibrosis and myonecrosis in mdx mice by suramin, a TGF-beta1 blocker. *Muscle Nerve*. 2011; 43: 82–7.
59. **Iwata Y, Katanosaka Y, Hisamitsu T, Wakabayashi S.** Enhanced Na+/H+exchange activity contributes to the pathogenesis of muscular dystrophy *via* involvement of P2 receptors. *Am J Pathol*. 2007; 171: 1576–87.